

Many-body quantum resources of graph states

Marcin Płodzień¹, Maciej Lewenstein^{1,2} and Jan Chwedeńczuk³

¹*ICFO-Institut de Ciències Fotoniques, The Barcelona Institute of Science and Technology, 08860 Castelldefels (Barcelona), Spain*

²*ICREA, Passeig Lluis Companys 23, 08010 Barcelona, Spain*

³*Faculty of Physics, University of Warsaw, ul. Pasteura 5, 02-093 Warszawa, Poland*

Characterizing the non-classical correlations of a complex many-body system is an important part of quantum technologies. A versatile tool for such a task is one that scales well with the size of the system and which can be both easily computed and measured. In this work we focus on graph states, that are promising platforms for quantum computation, simulation and metrology. We consider four topologies, namely the star graph states with edges, Turán graphs, r -ary tree graphs, and square grid cluster states, and provide a method to characterise their quantum content: the many-body Bell correlations, non-separability and entanglement depth for an arbitrary number of qubits. We also relate the strength of these many-body correlations to the usefulness of graph states for quantum sensing. Finally, we characterize many-body entanglement depth in graph states with up to 8 qubits in 146 classes non-equivalent under local transformations and graph isomorphisms. The technique presented is simple and does not make any assumptions about the multi-qubit state, so it could find applications wherever precise knowledge of many-body quantum correlations is required.

Introduction— Quantum coherence and many-body quantum correlations, such as entanglement or Bell correlations are the key features of many-body quantum systems [1–5]. In addition to their fundamental aspects, they are also seen as vital for future quantum-based technologies [6, 7]. To trigger the “second quantum revolution”, we must learn to prepare and store the many-body quantum states in a controlled way, and subsequently characterise and certify their quantum content.

In this context, an important family of many-body quantum systems are the graph states, with qubits placed at their nodes and connected by edges representing the two-body interactions. Graphs can have different topologies, resembling stars [Fig. 1(a)], stars with edges [Fig. 1(b)], Turán graph structure where nodes are partitioned into separated groups with no connections within each group [Fig. 1(c)], or tree-like fractals [Fig. 1(d)]. Some topologies, such as cluster graphs, see Fig. 1(e), enable universal quantum computation through a series of local measurements and classical feedforward operations, known as measurement-based quantum computing [8–15]. Graph states have been studied as a resource for quantum communication [16–28], and more recently for quantum metrology [29]. Each graph state belongs to an equivalence class under local Clifford operations [30–32], so the optimal preparation of graph states relates to finding the state orbit with the lowest number of qubit connections [33]. They have been prepared experimentally in a variety of physical platforms, including photonic systems [34–36], spin-1/2 systems [37], atomic ensembles [38–40], solid state systems such as quantum dots [41], and superconducting qubits [42].

Future applications require that we can characterise the “quantum content” of graph states: the strength and depth of the correlations and how they scale with system size. Once the quantum content of a graph state

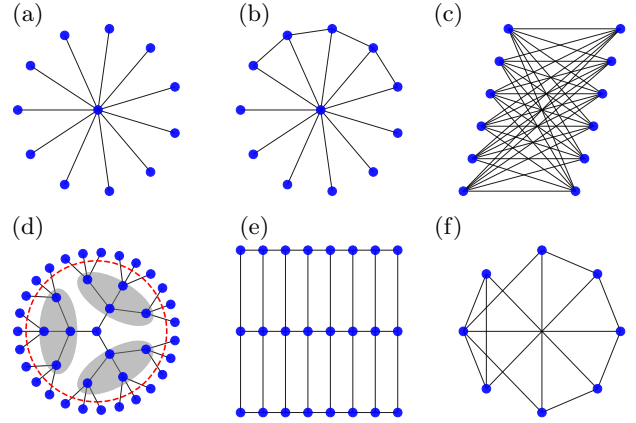


FIG. 1. Examples of distinct graph states topologies. (a) star graph with $L = 12$ nodes, (b) star graph with $L = 12$ nodes and $p = 4$ edges, (c) Turán graph with $L = 12$ nodes partitioned into equal $K = 2$ groups, (d) r -ary tree with $r = 3$ roots and $h = 2$ depth, (e) square grid graph size, and (f) eight-qubits graph state representative of one of 146 non-equivalent classes under local unitary transformations and graph isomorphisms.

is known, we should be able to tell how the correlations change when some edges are added or removed. Typically, the entanglement of graph states has been characterised by the Schmidt measure and geometric measures [43–46], or by the projector-based entanglement witness [47, 48]. The former defines the degree of entanglement by the supremum of the fidelities between the considered state and the set of all product states, and the latter refers to the overlap of the considered state with the Greenberg-Horne-Zeilinger (GHZ) state. The use of these entanglement measures has greatly expanded our understanding of graph states. However, they are not always easy to use—they can be difficult to calculate nu-

merically or are only applicable to a certain set of states.

In this work, we propose a new method for characterizing the quantum content of graph states that satisfies the following criteria: (i) it does not rely on the distance in the Hilbert space, thus it is easily computable; (ii) it tells directly how the quantum correlations change when the graph connectivity changes; (iii) it is experimentally accessible; (iv) it can be applied to both pure and mixed states, which is particularly important when the coupling gates are imperfect.

The method requires knowledge of a single element of the density matrix of the graph. From this object one can infer the depth of entanglement and many-body Bell correlations [49–55]. The method is scalable in two ways. First, it applies to graph states of arbitrary size. Second, it allows for a systematic study of how the strength of correlations changes as the interactions between the qubits (i.e., the edges) are modified, providing control over the quantum resources required for a particular task. In addition, the aforementioned matrix element used by this method is experimentally accessible by measuring of the multiple quantum coherences [56, 57].

We discuss applications of the proposed method for four graph topologies, i.e., star graphs, Turán graphs, r -ary tree graphs and cluster states [58], and for 146 non-equivalent classes of graph states with up to $L = 8$ qubits with respect to local unitary transformations and graph isomorphisms. We provide analytical results for the amount of quantum correlations for any number of qubits. Finally, we indicate the quantum-enhanced metrological utility of these graphs.

Preliminaries— A graph G is a pair $G = (V, E)$, where V is set of $|V|$ nodes, while E is a set of $|E|$ edges connecting any two nodes $(k, l) \in E$, $k, l \in V$. A graph state $|\psi\rangle$ is defined on a graph G as following: each node $v_k \in V$ corresponds to a qubit in a eigenstate of $\hat{\sigma}_x$ operator with $+1$ eigenvalue, while edge (k, l) corresponds to action of a Control-Z gate $\hat{C}_z^{(kl)}$ between nodes k and l , i.e. $|\psi\rangle = \prod_{(k,l) \in E(G)} \hat{C}_z^{(kl)} |\psi_{\text{ini}}\rangle$, $|\psi_{\text{ini}}\rangle = \bigotimes_{k=1}^L |0_x^{(k)}\rangle$, where, $\hat{\sigma}_x^{(k)} |0_x^{(k)}\rangle = +1 |0_x^{(k)}\rangle$, $\hat{C}_z^{(kl)} = |00\rangle\langle 00|_z + |01\rangle\langle 01|_z + |10\rangle\langle 10|_z - |11\rangle\langle 11|_z$, with $|00\rangle_z = |0_z^{(k)}\rangle \otimes |0_z^{(l)}\rangle$. Quantum correlations stem from interactions represented as a pattern of edges.

To certify the quantum content of a given graph state, we use the many-body quantum correlator considered in [59–68], namely

$$\mathcal{E}_L^{(q)}[\hat{\rho}] = \max_{\vec{\kappa}} \left| \text{Tr} \left[\hat{\rho} \bigotimes_{k=1}^L \hat{\sigma}_{+, \kappa_k}^{(k)} \right] \right|^2, \quad (1)$$

where $\vec{\kappa} = \{\kappa_1, \dots, \kappa_L\}$ is a vector of orientations of rising operators $\hat{\sigma}_{+, \kappa_k}^{(k)}$, $\kappa = x, y, z$, eg. $\hat{\sigma}_{+, z}^{(k)} = 1/2(\hat{\sigma}_x^{(k)} + i\hat{\sigma}_y^{(k)})$. The optimal $\vec{\kappa}$, such that maximizes $\mathcal{E}_L^{(q)}$, we denote as $\vec{\kappa}^*$. The versality of this correlator stems from

the fact that when

$$\mathcal{E}_L^{(q)}[\hat{\rho}] \leq 4^{-L} \quad \text{or} \quad \mathcal{E}_L^{(q)}[\hat{\rho}] \leq 2^{-L} \quad (2)$$

the correlations can be reproduced, respectively, either with a fully separable state or a local hidden-variable theory. Violation of the former inequality certifies the many-body entanglement while the breaking of the latter signals the presence of many-body Bell correlations [69].

The many-body correlations characterized by $\mathcal{E}_L^{(q)}$ are useful for quantum-enhanced metrology [61]. According to the Cramer-Rao theorem, the quantum Fisher information [70], that sets the lower bound for the sensitivity of estimation of the phase θ through $\Delta^2\theta \geq \mathcal{F}^{-1}[\hat{\rho}]$, satisfies [61]

$$\mathcal{F}[\hat{\rho}] \geq 4L^2 \mathcal{E}_L^{(q)}[\hat{\rho}], \quad (3)$$

In particular, the maximal value of the $\mathcal{E}_L^{(q)} = 4^{-1}$ provided by the GHZ state, gives the sensitivity at the Heisenberg limit, i.e., $\mathcal{F}[\hat{\rho}] = L^2$ [71].

In the following, we use a convenient parametrization

$$\mathcal{E}_L^{(q)}[\hat{\rho}] = 4^{-(1+\gamma)}, \quad (4)$$

where the exponent $\gamma \geq 0$ depends on state $\hat{\rho}$, and $\gamma = 0$ for GHZ states. The larger value of γ , the weaker are the many-body correlations. The entanglement criterion and the Bell inequality, see Eq. (2), become respectively

$$\gamma < L - 1 \quad \text{and} \quad \gamma < \frac{L}{2} - 1. \quad (5)$$

Apart from certifying the entanglement and Bell correlations, $\mathcal{E}_L^{(q)}$, and thus γ , carries information about their depth [59, 69]. When γ fulfills

$$\nu + 1 > \gamma \geq \nu \quad (6)$$

for a given $\nu \in \mathbb{N}$, then the system is $(L - \nu)$ -partite entangled (for example, when $\gamma > L - 1$, $\hat{\rho}$ is separable). Similarly, when

$$\frac{\nu + 1}{2} > \gamma \geq \frac{\nu}{2}, \quad (7)$$

then at least $L - \nu$ particles are Bell-correlated. Finally, when

$$\gamma < \log_4 L, \quad (8)$$

then according to Eq. (3), $\mathcal{F}[\hat{\rho}] > L$, giving the sub shot-noise sensitivity of the phase estimation, i.e., $\Delta^2\theta < L^{-1}$.

In the following, we use exponent γ as a tool to study quantum resources of graph states and to demonstrate their potential for quantum-enhanced metrology.

Results: The star graph — We start with a star graph and analyze how the quantum correlations characterized

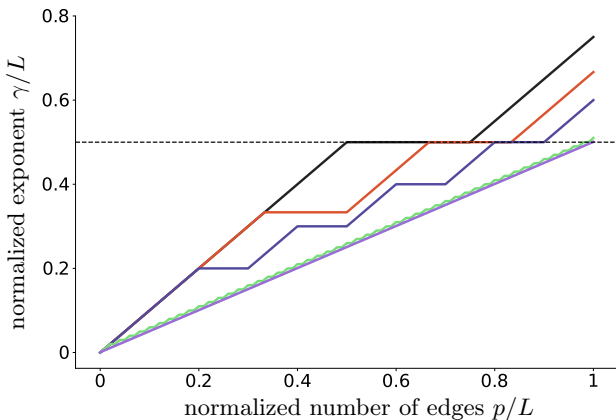


FIG. 2. The normalized exponent γ/L for a star graph with edges, Fig. 1(b), as a function of the number of edges p normalized to L . The colors correspond to: $L = 4$ (black), $L = 6$ (orange), $L = 10^1$ (blue), $L = 10^2$ (green) and $L = 10^3$ (purple). The dashed horizontal line denotes the Bell limit. All the values of $\gamma/L < 1$ imply many-body entanglement and when $\gamma/L < 1/2$ the many-body Bell correlations are present.

by $\mathcal{E}_L^{(q)}$ depend on the number of connections between the nodes. The starting setup consists of a central node connected with all the other but with no borders linking the corona nodes, see Fig. 1(a). For L qubits, this configuration corresponds to the GHZ state with the optimal direction given by $\vec{\kappa}^* = \{z_1, x_2 \dots x_L\}$, i.e.

$$|\psi\rangle = \frac{1}{\sqrt{2}} \left(|0_z^{(1)} 0_x^{(2)} 0_x^{(3)} \dots\rangle + |1_z^{(1)} 1_x^{(2)} 1_x^{(3)} \dots\rangle \right). \quad (9)$$

Hence $\gamma = 0$, the entanglement and Bell correlations are fully L -partite, and Eq. (9) is the reference state for quantum metrology. We now show that the addition of edges to the star leads to the degradation of quantum correlations. The first border connection couples the second and the third qubit via \hat{C}_z^{23} and transforms $|0_x^{(2)} 0_x^{(3)}\rangle$ and $|1_x^{(2)} 1_x^{(3)}\rangle$ of the state (9) into

$$|0_x^{(2)} 0_x^{(3)}\rangle \longrightarrow \frac{1}{\sqrt{2}} \left(|0_y^{(2)} 0_y^{(3)}\rangle + i |1_y^{(2)} 1_y^{(3)}\rangle \right) e^{-i\frac{\pi}{4}} \quad (10a)$$

$$|1_x^{(2)} 1_x^{(3)}\rangle \longrightarrow \frac{1}{\sqrt{2}} \left(|0_y^{(2)} 0_y^{(3)}\rangle - i |1_y^{(2)} 1_y^{(3)}\rangle \right) e^{i\frac{\pi}{4}}. \quad (10b)$$

As such, the dominant GHZ component is

$$|\psi\rangle = \frac{1}{2} \left(|0_z^{(1)} 0_y^{(2)} 0_y^{(3)} 0_x^{(4)} \dots\rangle + i |1_z^{(1)} 1_y^{(2)} 1_y^{(3)} 1_x^{(4)} \dots\rangle + \dots \right), \quad (11)$$

hence the new optimal direction changes to $\vec{\kappa}^* = \{z_1, y_2, y_3, x_4, \dots, x_L\}$, and $\gamma = 1$. Therefore, the entanglement- and nonlocality-depth, compared to Eq. (9), have dropped by either one party or two parties, see Eqs (5) and (6) respectively. When analyzing the subsequent couplings we always identify the dominant GHZ component. Next, providing the additional connection

between third and fourth qubit via the $\hat{C}_z^{(34)}$ the new optimal direction changes $\vec{\kappa}^* = \{z_1, y_2, y_3, x_4, \dots, x_L\} \rightarrow \vec{\kappa}^* = \{z_1, z_2, x_3, z_4, x_5, \dots, x_L\}$, and $\gamma = 2$. Consecutive couplings modify the optimal bases only for the pair of newly coupled nodes. For instance, the next two links results in the optimal $\vec{\kappa}^* = \{z_1, z_2, x_3, z_4, z_5, x_6, \dots, x_L\}$, and $\gamma = 3$. From now on, the pattern is established: when a connection is added to an even number of links, γ always grows by one. When added to an odd number of connections, γ remains unchanged. Interestingly, the closing connection either keeps γ constant (for L even) or increases it by 1 (if L is odd). This general analysis allows us to predict the strength of quantum correlations in any star graph state [69].

In Fig. 2, we show how the exponent γ , normalized to L , changes with the growing number of established borders, using $L = 4, 6, 10, 100, 1000$. The number of borders p is normalized to L , giving $x = p/L$, namely the fraction of edges. While for small L , the Bell correlations vanish (i.e., $\gamma/L > \frac{1}{2}$), in the quasi-thermodynamical limit (here we used $L = 1000$ and checked that the curves do not change for higher L 's) the many-body correlations are present for all star graph states. Moreover, for large L we can analytically predict the depth of many-body Bell correlations and entanglement. Since, starting from $p = 4$ edges, the γ grows by one only every second p , then the coherence behaves like $\gamma \simeq \frac{p}{2}$. According to Eq. (8), all graphs with $p < 2 \log_4 L$ are useful for quantum metrology. Also, one now can calculate the depth of entanglement and Bell correlations in the graph state. For instance, for $L = 128$ and half of the nodes connected, i.e., $p = L/2$, we obtain $\gamma \simeq L/4$, thus the entanglement extends over $L - \gamma = 96$ qubits and the Bell correlations encompass $L - 2\gamma = 64$ of them, see Eqs (5) and (6), respectively.

The Turán graph—Next, we consider the Turán graphs topology, and indicate their usefulness for quantum metrology. The Turán graph is defined via the following construction: L nodes are partitioned into K groups, each group has n_k nodes, $\sum_{k=1}^K n_k = L$. Two nodes are connected only if they do not belong to the same group [58], see Fig. 1(c). A special case of Turán graph, is a star graph with $K = 2$ groups, where $n_1 = 1$, and $n_2 = L - 1$. Considering symmetric partitioning of nodes into K the number of edges reads $|E| = (1 - \frac{1}{K}) \frac{L^2 - s^2}{2} + \binom{s}{2}$, where s is remainder of division L/K . For fixed L , number of necessary \hat{C}_z gates increases with number of groups K .

With the exact many-body calculations, we revealed that for graph states of K groups, with at least two qubits in each group, $n_k \geq 2$ for $k = 1 \dots K$, the exponent has the simple form $\gamma = K - 1$ with corresponding $\vec{\kappa}^* = \{x_1, \dots, x_L\}$. As such, the entanglement- and nonlocality-depth, with respect to the ideal GHZ state, drop with an increasing number of groups K , see Eqs (5) and (6). Nevertheless, the fact that γ depends only on K , and not on L , indicates that graph states with Turán

graph topology are a valuable resource for quantum-enhanced metrology, see Eq. (8), i.e. $K < \log_4 L + 1$ for sufficiently large L . We note that *bundle graphs* introduced in Ref.[29] are in fact Turán graphs.

The r -ary tree graph— In the following, we show how the method works for another prominent topology, i.e., the r -ary tree graphs [58]. These are characterized by the number of connections that stem from each node, r , and the distance between the center and the most distant node, h , see Fig. 1(d). Since the number of nodes for the k -th layer is r^k , the total number L is

$$L(r, h) = \sum_{k=0}^h r^k = \frac{1 - r^{h+1}}{1 - r}. \quad (12)$$

The analysis of quantum correlations in this system is most efficient when first considering subsystems of star graphs, denoted by shaded areas in Fig. 1(d). Each such star graph, when disregarding its connections to other layers, forms a GHZ state

$$|\psi_k\rangle = \frac{1}{\sqrt{2}}(|0_z\rangle|0_x\rangle^{\otimes r^{k+1}} + |1_z\rangle|1_x\rangle^{\otimes r^{k+1}}). \quad (13)$$

There are r^k such GHZ states for the the k^{th} layer, formed at every second k , i.e., for $k = 1, 3, 5, \dots$. Tree graphs with even and odd r and h should be considered separately because each coupling of the $|1_z\rangle$ component of the $(k+2)^{\text{th}}$ GHZ state flips the $|1_x\rangle$'s of the k^{th} one. If r is even (e), these flippings bring the state back to $|1_x\rangle$ while if it is odd (o), the outcome is $|0_x\rangle$. This drastically reduces the GHZ coherence, giving respectively for even h

$$\gamma_e = r \frac{r^h - 1}{r^2 - 1}, \quad \gamma_o = \frac{r^h - 2r + 1}{r - 1}. \quad (14)$$

Because the growth of $\gamma_{e,o}$ with r, h is smaller than growth of total number of nodes $L(r, h)$, Eq.(12), we conclude that multi-branch trees are characterized by very high depth of multi-partite entanglement and Bell correlations, see Eqs (5) and (6). Addition of another layer $h \rightarrow h + 1$, that does not form a set of GHZ states [those nodes outside the red dashed circle in Fig. 1(d)], does not change the GHZ coherence of the tree graph. Hence, expressions for $\gamma_{e/o}$ hold [69]. Crucially, in the even- r case, the depth of quantum correlations is macroscopic, as $\gamma_e/L(r, h) \simeq 1$ for large r or h . When r is odd $\gamma_o/L(r, h) \simeq r^{-2}$ which is small for large r . In both cases, according to Eqs (5) and (6), the entanglement and Bell correlations extend over the most of the system.

Cluster states— Cluster states contain resources for measurement based quantum computations [8–15]. We considered cluster states on a $m \times n$ square lattice, see Fig. 1(e). Exact numerical calculation reveals linear scaling of entanglement and Bell correlations with number of qubits $L = nm$, namely $\gamma = n + 1$ for $m = 2$, $\gamma = 2n - 2$ for $m = 3$.

Non-equivalent classes of graph states under local unitaries— Quantum correlations cannot be changed by any local unitary (LU) transformation, thus value of γ is independent on LU, or local graph complementation [30–32]. As a last example we characterize quantum correlations for 146 non-equivalent classes, an example of which is shown in Fig. 1(f), under local complementation and graph isomorphism for states with $L \leq 8$ qubits [72–74], see [69].

Conclusions— We have developed a method allowing the characterisation of quantum resources of graph states, such as the many-body entanglement and Bell correlations, and quantum Fisher information. For the considered examples of the star, Turán, and r -ary tree graphs topologies, we provided analytical predictions for the many-body entanglement depth and Bell correlations for any number of qubits. Moreover, we showed that Turán graph topology forms a family of many-body quantum states useful for quantum metrology. We used the method to analyze quantum correlations for square grid cluster states. Finally, we characterized 146 non-equivalent classes under local complementation and graph isomorphism for up to 8 qubits with respect to many-body entanglement depth.

The proposed method can be used for arbitrary topologies of graph states with a full many-body numerical approach, or with the help of tensor networks quantum state representation. Furthermore, it allows us to formulate the problem of graph state preparation with a desired entanglement depth as an optimization problem with constraints on qubits connectivity or on the amount of entangling gates.

Acknowledgements—JCh was supported by the National Science Centre, Poland, within the QuantERA II Programme that has received funding from the European Union's Horizon 2020 research and innovation program under Grant Agreement No 101017733, Project No. 2021/03/Y/ST2/00195.

ICFO group acknowledges support from: European Research Council AdG NOQIA; MCIN/AEI (PGC2018-0910.13039/501100011033, CEX2019-000910-S/10.13039/501100011033, Plan National FIDEUA PID2019-106901GB-I00, Plan National STAMEENA PID2022-139099NB, I00, project funded by MCIN/AEI/10.13039/501100011033 and by the "European Union NextGenerationEU/PRTR" (PRTR-C17.I1), FPI); QUANTERA MAQS PCI2019-111828-2; QUANTERA DYNAMITE PCI2022-132919, QuantERA II Programme co-funded by European Union's Horizon 2020 program under Grant Agreement No 101017733; Ministry for Digital Transformation and of Civil Service of the Spanish Government through the QUANTUM ENIA project call - Quantum Spain project, and by the European Union through the Recovery, Transformation and Resilience Plan - NextGenerationEU within the framework of the Digital Spain 2026 Agenda; Fundació

Cellex; Fundació Mir-Puig; Generalitat de Catalunya (European Social Fund FEDER and CERCA program, AGAUR Grant No. 2021 SGR 01452, QuantumCAT U16-011424, co-funded by ERDF Operational Program of Catalonia 2014-2020); Barcelona Supercomputing Center MareNostrum (FI-2023-3-0024); Funded by the European Union.

Views and opinions expressed are however those of the author(s) only and do not necessarily reflect those of the European Union, European Commission, European Climate, Infrastructure and Environment Executive Agency (CINEA), or any other granting authority. Neither the European Union nor any granting authority can be held responsible for them (HORIZON-CL4-2022-QUANTUM-02-SGA PASQuanS2.1, 101113690, EU Horizon 2020 FET-OPEN OPTologic, Grant No 899794), EU Horizon Europe Program (This project has received funding from the European Union’s Horizon Europe research and innovation program under grant agreement No 101080086 NeQSTGrant Agreement 101080086 — NeQST); ICFO Internal “QuantumGaudi” project; European Union’s Horizon 2020 program under the Marie Skłodowska-Curie grant agreement No 847648; “La Caixa” Junior Leaders fellowships, La Caixa” Foundation (ID 100010434): CF/BQ/PR23/11980043.

-
- [1] A. Streltsov, G. Adesso, and M. B. Plenio, *Rev. Mod. Phys.* **89**, 041003 (2017).
- [2] R. Horodecki, P. Horodecki, M. Horodecki, and K. Horodecki, *Rev. Mod. Phys.* **81**, 865 (2009).
- [3] N. Brunner, D. Cavalcanti, S. Pironio, V. Scarani, and S. Wehner, *Rev. Mod. Phys.* **86**, 419 (2014).
- [4] A. K. Srivastava, G. Müller-Rigat, M. Lewenstein, and G. Rajchel-Mieldzióć, Introduction to quantum entanglement in many-body systems, in *New Trends and Platforms for Quantum Technologies* (Springer Nature Switzerland, 2024) p. 225–285.
- [5] P. Horodecki, Łukasz Rudnicki, and K. Życzkowski, Multipartite entanglement (2024), arXiv:2409.04566 [quant-ph].
- [6] E. Chitambar and G. Gour, *Rev. Mod. Phys.* **91**, 025001 (2019).
- [7] R. Salazar, J. Czartowski, R. R. Rodríguez, G. Rajchel-Mieldzióć, P. Horodecki, and K. Życzkowski, Quantum resource theories beyond convexity (2024).
- [8] R. Jozsa, NATO Science Series, III: Computer and Systems Sciences. *Quantum Information Processing-From Theory to Experiment* **199**, 137 (2006).
- [9] R. Raussendorf and H. J. Briegel, *Phys. Rev. Lett.* **86**, 5188 (2001).
- [10] R. Raussendorf, D. E. Browne, and H. J. Briegel, *Phys. Rev. A* **68**, 022312 (2003).
- [11] D. W. Leung, *International Journal of Quantum Information* **02**, 33 (2004), <https://doi.org/10.1142/S0219749904000055>.
- [12] M. Hein, W. Dür, J. Eisert, R. Raussendorf, M. V. den Nest, and H. J. Briegel, Entanglement in graph states and its applications (2006), arXiv:quant-ph/0602096 [quant-ph].
- [13] D. Gross and J. Eisert, *Phys. Rev. Lett.* **98**, 220503 (2007).
- [14] H. J. Briegel, D. E. Browne, W. Dür, R. Raussendorf, and M. Van den Nest, *Nature Physics* **5**, 19 (2009).
- [15] M. A. Raza, A. N. Alahmadi, W. Basaffar, D. G. Glynn, M. K. Gupta, J. W. P. Hirschfeld, A. N. Khan, H. Shoaih, and P. Solé, *Mathematics* **11**, 2310 (2023).
- [16] M. Cuquet and J. Calsamiglia, *Phys. Rev. A* **86**, 042304 (2012).
- [17] J. Javelle, M. Mhalla, and S. Perdrix, New protocols and lower bounds for quantum secret sharing with graph states, in *Theory of Quantum Computation, Communication, and Cryptography* (Springer Berlin Heidelberg, 2013) p. 1–12.
- [18] B. A. Bell, D. Markham, D. A. Herrera-Martí, A. Marin, W. J. Wadsworth, J. G. Rarity, and M. S. Tame, *Nature Communications* **5**, 10.1038/ncomms6480 (2014).
- [19] C. Meignant, D. Markham, and F. Grosshans, *Phys. Rev. A* **100**, 052333 (2019).
- [20] F. Hahn, A. Pappa, and J. Eisert, *npj Quantum Information* **5**, 10.1038/s41534-019-0191-6 (2019).
- [21] P. Hilaire, E. Barnes, and S. E. Economou, *Quantum* **5**, 397 (2021).
- [22] Y. Ding, Y. Wei, Z. Li, and M. Jiang, *Quantum Information Processing* **22**, 10.1007/s11128-023-04157-0 (2023).
- [23] A. Fischer and D. Towsley, in *2021 IEEE International Conference on Quantum Computing and Engineering (QCE)* (IEEE, 2021) p. 324–333.
- [24] A. Unnikrishnan and D. Markham, *Physical Review A* **105**, 10.1103/physreva.105.052420 (2022).
- [25] U. I. Meyer, F. Grosshans, and D. Markham, *Phys. Rev. A* **108**, 012402 (2023).
- [26] B. Li, K. Goodenough, F. Rozpędek, and L. Jiang, Generalized quantum repeater graph states (2024).
- [27] O. Makuta, L. T. Ligthart, and R. Augusiak, *npj Quantum Information* **9**, 10.1038/s41534-023-00789-3 (2023).
- [28] B. Li, K. Goodenough, F. Rozpędek, and L. Jiang, Generalized quantum repeater graph states (2024), arXiv:2407.01429 [quant-ph].
- [29] N. Shettell and D. Markham, *Phys. Rev. Lett.* **124**, 110502 (2020).
- [30] A. Bouchet, *Discrete Mathematics* **114**, 75 (1993).
- [31] M. Van den Nest, J. Dehaene, and B. De Moor, *Phys. Rev. A* **69**, 022316 (2004).
- [32] J. C. Adcock, S. Morley-Short, A. Dahlberg, and J. W. Silverstone, *Quantum* **4**, 305 (2020).
- [33] A. Cabello, L. E. Danielsen, A. J. López-Tarrida, and J. R. Portillo, *Phys. Rev. A* **83**, 042314 (2011).
- [34] A. Russo, E. Barnes, and S. E. Economou, *New Journal of Physics* **21**, 055002 (2019).
- [35] P. Thomas, L. Ruscio, O. Morin, and G. Rempe, *Nature* **629**, 567–572 (2024).
- [36] Z. Raissi, E. Barnes, and S. E. Economou, *PRX Quantum* **5**, 020346 (2024).
- [37] X. X. Li, D. X. Li, and X. Q. Shao, *Phys. Rev. A* **109**, 042604 (2024).
- [38] S. R. Clark, C. M. Alves, and D. Jaksch, *New Journal of Physics* **7**, 124–124 (2005).
- [39] D. Ballester, J. Cho, and M. S. Kim, *Phys. Rev. A* **83**, 010302 (2011).
- [40] E. S. Cooper, P. Kunkel, A. Periwal, and M. Schleier-Smith, *Nature Physics* **20**, 770–775 (2024).

- [41] J.-P. Li, J. Qin, A. Chen, Z.-C. Duan, Y. Yu, Y. Huo, S. Höfling, C.-Y. Lu, K. Chen, and J.-W. Pan, *ACS Photonics* **7**, 1603–1610 (2020).
- [42] K. Gnatenko and V. Tkachuk, *Physics Letters A* **396**, 127248 (2021).
- [43] D. Markham, A. Miyake, and S. Virmani, *New Journal of Physics* **9**, 194–194 (2007).
- [44] J. Eisert and H. J. Briegel, *Phys. Rev. A* **64**, 022306 (2001).
- [45] Q.-Q. Guo, X.-Y. Chen, and Y.-Y. Wang, *Chinese Physics B* **23**, 050309 (2014).
- [46] M. Hajdušek and M. Muraio, *AIP Conference Proceedings* **1633**, 168 (2014), https://pubs.aip.org/aip/acp/article-pdf/1633/1/168/12136622/168_1_online.pdf.
- [47] G. Tóth and O. Gühne, *Phys. Rev. Lett.* **94**, 060501 (2005).
- [48] R. Zander and C. K.-U. Becker, Benchmarking multipartite entanglement generation with graph states (2024), arXiv:2402.00766 [quant-ph].
- [49] M. Żukowski and Č. Brukner, *Phys. Rev. Lett.* **88**, 210401 (2002).
- [50] N. D. Mermin, *Phys. Rev. Lett.* **65**, 1838 (1990).
- [51] N. D. Mermin, *American Journal of Physics* **49**, 940 (1981), https://pubs.aip.org/aapt/ajp/article-pdf/49/10/940/11864850/940_1_online.pdf.
- [52] E. G. Cavalcanti, C. J. Foster, M. D. Reid, and P. D. Drummond, *Phys. Rev. Lett.* **99**, 210405 (2007).
- [53] M. D. Reid, Q.-Y. He, and P. D. Drummond, *Frontiers of Physics* **7**, 72 (2012).
- [54] E. Cavalcanti, Q. He, M. Reid, and H. Wiseman, *Phys. Rev. A* **84**, 032115 (2011).
- [55] M. Ardehali, *Physical Review A* **46**, 5375 (1992).
- [56] M. Gärttner, J. G. Bohnet, A. Safavi-Naini, M. L. Wall, J. J. Bollinger, and A. M. Rey, *Nature Physics* **13**, 781 (2017).
- [57] M. Gärttner, P. Hauke, and A. M. Rey, *Phys. Rev. Lett.* **120**, 040402 (2018).
- [58] J. Bondy and U. Muny, *Graph theory with applications* (The Macmillan Press, London, 1976).
- [59] A. Niezgoda, M. Panfil, and J. Chwedeńczuk, *Phys. Rev. A* **102**, 042206 (2020).
- [60] M. Płodzień, M. Kościelski, E. Witkowska, and A. Sinatra, *Phys. Rev. A* **102**, 013328 (2020).
- [61] A. Niezgoda and J. Chwedeńczuk, *Phys. Rev. Lett.* **126**, 210506 (2021).
- [62] M. Płodzień, M. Lewenstein, E. Witkowska, and J. Chwedeńczuk, *Phys. Rev. Lett.* **129**, 250402 (2022).
- [63] M. Dziurawiec, T. Hernández Yanes, M. Płodzień, M. Gajda, M. Lewenstein, and E. Witkowska, *Phys. Rev. A* **107**, 013311 (2023).
- [64] T. Hernández Yanes, G. Žlabys, M. Płodzień, D. Burba, M. M. Sinkevičienė, E. Witkowska, and G. Juzeliūnas, *Phys. Rev. B* **108**, 104301 (2023).
- [65] M. Płodzień, T. Wasak, E. Witkowska, M. Lewenstein, and J. Chwedeńczuk, *Phys. Rev. Res.* **6**, 023050 (2024).
- [66] D. A. Hamza and J. Chwedeńczuk, *Phys. Rev. A* **110**, 012210 (2024).
- [67] M. Płodzień, J. Chwedeńczuk, M. Lewenstein, and G. Rajchel-Mieldzioc, *Phys. Rev. A* **110**, 032428 (2024).
- [68] M. Płodzień, J. Chwedeńczuk, and M. Lewenstein, Inherent quantum resources in the stationary spin chains (2024), arXiv:2405.16974 [quant-ph].
- [69] See the Supplementary materials for the detailed step-by-step derivation and discussion (2024).
- [70] S. L. Braunstein and C. M. Caves, *Phys. Rev. Lett.* **72**, 3439 (1994).
- [71] L. Pezzé and A. Smerzi, *Phys. Rev. Lett.* **102**, 100401 (2009).
- [72] M. Hein, J. Eisert, and H. J. Briegel, *Phys. Rev. A* **69**, 062311 (2004).
- [73] A. Cabello, A. J. López-Tarrida, P. Moreno, and J. R. Portillo, *Physics Letters A* **373**, 2219–2225 (2009).
- [74] A. Cabello, A. J. López-Tarrida, P. Moreno, and J. R. Portillo, *Phys. Rev. A* **80**, 012102 (2009).

MANY-BODY CORRELATOR $\mathcal{E}_L^{(q)}$

Suppose a system of L parties each giving a pair of binary outcomes $\sigma_{n_k}^{(k)} = \pm 1$ and $\sigma_{n'_k}^{(k)} = \pm 1$ ($k \in \{1 \dots L\}$). Next, we consider the correlation function $\mathcal{E}_L = |\langle \sigma_+^{(1)} \dots \sigma_+^{(L)} \rangle|^2$, where $\sigma_+^{(k)} = 1/2(\sigma_{n_k}^{(k)} + i\sigma_{n'_k}^{(k)})$, where the average $\langle \cdot \rangle$ is taken over many experimental realizations. If this average can be reproduced with a theory satisfying the postulates of local realism, then

$$\langle \sigma_+^{(1)} \dots \sigma_+^{(L)} \rangle = \int d\lambda p(\lambda) \prod_{k=1}^L \sigma_+^{(k)}(\lambda), \quad (\text{S.1})$$

where $p(\lambda)$ is a probability distribution of a random variable. Since $|\sigma_+^{(k)}(\lambda)|^2 = 1/2$, the Cauchy-Schwarz inequality (CSI) yields

$$\mathcal{E}_L \leq \int d\lambda p(\lambda) \prod_{k=1}^L |\sigma_+^{(k)}(\lambda)|^2 = 2^{-L}. \quad (\text{S.2})$$

As such, we conclude that

$$\mathcal{E}_L \leq 2^{-L} \quad (\text{S.3})$$

is the L -body Bell inequality, because its violation defies the postulates of local realism. When the parties are quantum two-level object, $\sigma_+^{(k)}$'s are replaced with the rising Pauli operators, giving

$$\mathcal{E}_L^{(q)}[\hat{\rho}] = |\text{Tr} \left[\hat{\rho} \bigotimes_{k=1}^L \hat{\sigma}_+^{(k)} \right]|^2. \quad (\text{S.4})$$

If $\hat{\rho}$ is fully separable, $\hat{\rho} = \int d\lambda p(\lambda) \bigotimes_{k=1}^L \hat{\rho}^{(k)}(\lambda)$, then using the upper bound $|\text{Tr} [\hat{\rho}^{(k)}(\lambda) \hat{\sigma}_+^{(k)}]|^2 \leq 4^{-1}$ and the CSI we obtain

$$\mathcal{E}_L^{(q)}[\hat{\rho}] \leq 4^{-L}. \quad (\text{S.5})$$

Considering the fact, that $\mathcal{E}_L^{(q)}$ contains L -fold action of rising operators, eventually the value of the correlator corresponds to a modulus square of the GHZ coherence between the components $|0\rangle^{\otimes L}$ and $|1\rangle^{\otimes L}$ of a quantum state. Hence, the GHZ state

$$|\psi\rangle_{\text{GHZ}} = \frac{1}{\sqrt{2}}(|1\rangle^{\otimes L} + |0\rangle^{\otimes L}), \quad (\text{S.6})$$

maximizes its value giving $\mathcal{E}_L^{(q)}[|\psi\rangle\langle\psi|] = 4^{-1}$. In general, for a given quantum state $\hat{\rho}$, the rising operators can be realized in distinct directions, independently for each spin, thus we use definition in Eq.(1).

STAR GRAPHS

From the point of view of the subsequent analysis it is important to list the following relations

$$\hat{C}_z |0_x 0_x\rangle = \frac{1}{\sqrt{2}}(|0_z 0_x\rangle + |1_z 1_x\rangle) \quad (\text{S.7a})$$

$$\hat{C}_z |1_x 0_x\rangle = \frac{1}{\sqrt{2}}(|0_z 0_x\rangle - |1_z 1_x\rangle) \quad (\text{S.7b})$$

$$\hat{C}_z |0_x 1_x\rangle = \frac{1}{\sqrt{2}}(|0_z 1_x\rangle + |1_z 1_x\rangle) \quad (\text{S.7c})$$

$$\hat{C}_z |1_x 1_x\rangle = \frac{1}{\sqrt{2}}(|0_z 1_x\rangle - |1_z 0_x\rangle). \quad (\text{S.7d})$$

Hence the connection of a pair of nodes that are in the eigen-states of the x operators yields an extra $1/\sqrt{2}$, which decreases the GHZ coherence. To contrary the coupling when one of the nodes in the the eigenstate of x and the other in the eigenstate of z does not produce such terms, namely

$$\hat{C}_z|0_z0_x\rangle = |0_z0_x\rangle \quad (\text{S.8a})$$

$$\hat{C}_z|0_z1_x\rangle = |0_z0_x\rangle \quad (\text{S.8b})$$

$$\hat{C}_z|1_z0_x\rangle = |1_z1_x\rangle \quad (\text{S.8c})$$

$$\hat{C}_z|1_z1_x\rangle = |1_z0_x\rangle. \quad (\text{S.8d})$$

Pair of nodes in the eigenstates of z , for instance $|0_z0_x\rangle$ are eigenstates of \hat{C}_z with ± 1 eigen-values, hence also do not influence the GHZ coherence.

The starting point of the analysis is the star state, i.e. the zero-border GHZ state

$$|\psi\rangle = \frac{1}{\sqrt{2}} \left(|0_z^{(1)}0_x^{(2)}0_x^{(3)} \dots\rangle + |1_z^{(1)}1_x^{(2)}1_x^{(3)} \dots\rangle \right), \quad (\text{S.9})$$

with the optimal direction $\vec{\kappa}^* = \{z_1, x_2, \dots, x_L\}$. The first connection via $\hat{C}_z^{(12)}$ gate yields

$$|\psi\rangle = \frac{1}{2} \left(|0_z^{(1)}\rangle(|0_y^{(2)}0_y^{(3)}\rangle + i|1_y^{(2)}1_y^{(3)}\rangle)e^{-i\frac{\pi}{4}}|0_x^{(4)} \dots\rangle + |1_z^{(1)}\rangle(|0_y^{(2)}0_y^{(3)}\rangle - i|1_y^{(2)}1_y^{(3)}\rangle)e^{i\frac{\pi}{4}}|1_x^{(4)} \dots\rangle \right). \quad (\text{S.10})$$

Note the $1/2$ prefactor, in contrast to $1/\sqrt{2}$ of the GHZ state. This is a consequence of the coupling of the x -axis eigenstates, see Eqs (S.7). The dominant GHZ coherence is related to the states $|0_z^{(1)}0_y^{(2)}0_y^{(3)}0_x^{(4)} \dots\rangle$ and $|1_z^{(1)}1_y^{(2)}1_y^{(3)}1_x^{(4)} \dots\rangle$ with the prefactor $1/2$, hence the new optimal direction $\vec{\kappa}^*$ and the exponent γ are equal to

$$\vec{\kappa}^* = \{z_1, y_2, y_3, x_4, \dots, x_L\} \quad (\text{S.11})$$

$$\gamma = 1 \quad (\text{S.12})$$

as reported in the main text.

The second border, i.e. $\hat{C}_z^{(23)}$ gate, generates the states that multiply the $|0_z^{(1)}\rangle$ and $|1_z^{(1)}\rangle$ of the central node as follows

$$|0_z^{(1)}\rangle : |0_z^{(2)}\rangle \frac{1}{\sqrt{2}} (|0_x^{(3)}0_z^{(4)}\rangle + |1_x^{(3)}1_z^{(4)}\rangle) + |1_z^{(2)}\rangle \frac{1}{\sqrt{2}} (|1_x^{(3)}0_z^{(4)}\rangle + |0_x^{(3)}1_z^{(4)}\rangle) \quad (\text{S.13a})$$

$$|0_z^{(0)}\rangle : |0_z^{(2)}\rangle \frac{1}{\sqrt{2}} (|0_x^{(3)}0_z^{(4)}\rangle - |1_x^{(3)}1_z^{(4)}\rangle) - |1_z^{(2)}\rangle \frac{1}{\sqrt{2}} (|0_x^{(3)}0_z^{(4)}\rangle - |1_x^{(3)}1_z^{(4)}\rangle). \quad (\text{S.13b})$$

Again the coupling of the first term from the first line with the last term of the second line gives the maximal GHZ coherence, hence

$$\vec{\kappa}^* = \{z_1, z_2, x_3, z_4, x_5, \dots, x_L\} \quad (\text{S.14})$$

$$\gamma = 2. \quad (\text{S.15})$$

From now on, we can only analyze the evolution of these two terms, namely $|0_z^{(1)}0_z^{(2)}0_x^{(3)}0_z^{(4)}\rangle|0_x\rangle^{\otimes L-4}$ versus $|1_z^{(1)}1_z^{(2)}1_x^{(3)}1_z^{(4)}\rangle|1_x\rangle^{\otimes L-4}$. And so, for three connections the dominant GHZ terms are

$$|0_z^{(1)}0_z^{(2)}0_x^{(3)}0_z^{(4)}\rangle|0_x\rangle^{\otimes L-4} \longrightarrow |0_z^{(1)}0_z^{(2)}0_x^{(3)}0_z^{(4)}0_x^{(5)}\rangle|0_x\rangle^{\otimes L-5} \quad (\text{S.16a})$$

$$|1_z^{(1)}1_z^{(2)}1_x^{(3)}1_z^{(4)}\rangle|1_x\rangle^{\otimes L-4} \longrightarrow |1_z^{(1)}1_z^{(2)}1_x^{(3)}1_z^{(4)}0_x^{(5)}\rangle|1_x\rangle^{\otimes L-5}. \quad (\text{S.16b})$$

To extract the GHZ coherence, the 5th node must be decomposed in some basis orthogonal to x , say z . This however produces a cost of an extra $1/\sqrt{2}$ term that decreases the coherence, which is now equal to

$$\vec{\kappa}^* = \{z_1, z_2, x_3, z_4, z_5, x_6, \dots, x_L\} \quad (\text{S.17})$$

$$\gamma = 3. \quad (\text{S.18})$$

Next, the 4th connection gives

$$|0_z^{(1)}0_z^{(2)}0_x^{(3)}0_z^{(4)}0_x^{(5)}\rangle|0_x\rangle^{\otimes L-5} \longrightarrow |0_z^{(1)}0_z^{(2)}0_x^{(3)}0_z^{(4)}0_x^{(5)}0_z^{(6)}\rangle|0_x\rangle^{\otimes L-6} \quad (\text{S.19a})$$

$$|1_z^{(1)}1_z^{(2)}1_x^{(3)}1_z^{(4)}0_x^{(5)}\rangle|1_x\rangle^{\otimes L-5} \longrightarrow |1_z^{(1)}1_z^{(2)}1_x^{(3)}1_z^{(4)}1_x^{(4)}1_z^{(5)}\rangle|1_x\rangle^{\otimes L-6}. \quad (\text{S.19b})$$

Now the extra rotation is not necessary. Hence although the coupling generated another $1/\sqrt{2}$ it is compensated by the lack of necessity to rotate the last node. This explains why the GHZ coherence,

$$\vec{\kappa}^* = \{z_1, z_2, x_3, z_4, x_5, z_6, x_7, \dots, x_L\} \quad (\text{S.20})$$

$$\gamma = 3 \quad (\text{S.21})$$

does not drop with respect to the three-connections case. From now on, the pattern is established, i.e., when n is even

$$\gamma_n = \gamma_{n-1}, \quad \vec{\kappa}^* = \{z_1, z_2, x_3, z_4, x_5, z_6, x_7, z_8, x_9, \dots, x_L\} \quad (\text{S.22a})$$

$$\gamma_{n+1} = 1 + \gamma_n, \quad \vec{\kappa}^* = \{z_1, z_2, x_3, z_4, x_5, z_6, x_7, z_8, x_9, x_{10}, \dots, x_L\}. \quad (\text{S.22b})$$

The closing connection couples the L^{th} with the 2nd one. According to the above arguments, when L is even this couples $|0_z^{(2)}\rangle$ with $|0_z^{(L)}\rangle$ and $|1_z^{(2)}\rangle$ with $|1_z^{(L)}\rangle$, which are the two-node eigenstates of the $\hat{C}_z^{(2L)}$ gate. Hence the the GHZ coherence does not change with respect to the previous step. However, if L is odd, the coupling is

$$|0_z^{(2)}0_x^{(L)}\rangle \longrightarrow |0_z^{(2)}0_x^{(L)}\rangle \quad (\text{S.23a})$$

$$|1_z^{(2)}0_x^{(L)}\rangle \longrightarrow |1_z^{(2)}1_x^{(L)}\rangle. \quad (\text{S.23b})$$

hence the coherence grows by a factor 4, i.e., γ drops by one, since no additional change of basis for the L^{th} node is now required. The optimal direction of spin rising operators has the alternating structure, namely

$$\vec{\kappa}^* = \{z_1, z_2, x_3, z_4, x_5, \dots, z_{L-1}, x_L\}. \quad (\text{S.24})$$

TREES

Here we provide the general formulæ for the correlator for any number of connectors r and any distance h . This however can be done by considering the parity of each parameter separately.

• h even, r odd

When r is odd, the first layer of r GHZ states coupling to the central node gives

$$|\psi\rangle = \frac{1}{\sqrt{2}^r} (|0_x^{(1)}\rangle|0_z\rangle^{\otimes r}|0_x\rangle^{\otimes r^2} + |1_x^{(1)}\rangle|1_z\rangle^{\otimes r}|1_x\rangle^{\otimes r^2}). \quad (\text{S.25})$$

Since r is odd, the coupling of the next layer will flip all the $|1_x\rangle$ of the previous layer, giving the dominant term

$$|\psi\rangle = \frac{1}{\sqrt{2}^{r+r^3}} (|0_x^{(1)}\rangle|0_z\rangle^{\otimes(r+r^3)}|0_x\rangle^{\otimes r^4} + |1_x^{(1)}\rangle|1_z\rangle^{\otimes(r+r^3)}|1_x\rangle^{\otimes r^4} + \dots)|0_x\rangle^{\otimes r^2}. \quad (\text{S.26})$$

As h is even, the procedure ends with another complete layer, but the last $|1_x\rangle$'s have no more layers to couple to and flip into $|0_x\rangle$, hence the full state takes the form (we list the dominant GHZ components)

$$|\psi\rangle = \frac{1}{\sqrt{2}^{r+r^3+\dots+r^{h-1}}} (|0_x^{(1)}\rangle|2_z\rangle^{\otimes(r+r^3+\dots+r^{h-1})}|0_x\rangle^{\otimes r^h} + |1_x^{(1)}\rangle|1_z\rangle^{\otimes(r+\dots+r^{h-1})}|1_x\rangle^{\otimes r^h})|0_x\rangle^{\otimes(r^2+\dots+r^{h-2})}. \quad (\text{S.27})$$

Hence the exponent γ reads

$$\gamma = -1 + r + r^2 + r^3 + \dots + r^{h-1} \quad (\text{S.28})$$

• h even, r even

When r is even, the first coupling gives

$$|\psi\rangle = \frac{1}{\sqrt{2}^r} (|0_x^{(1)}\rangle(|0_z\rangle^{\otimes r}|0_x\rangle^{\otimes r^2} + |1_z\rangle^{\otimes r}|1_x\rangle^{\otimes r^2})). \quad (\text{S.29})$$

Since r is now even, the coupling of the next layer does not flip the $|1_x\rangle$'s of the previous layer, and the dominant term now reads

$$|\psi\rangle = \frac{1}{\sqrt{2}^{r+r^3}} (|0_x^{(1)}\rangle|0_z\rangle^{\otimes(r+r^3)}|0_x\rangle^{\otimes(r^2+r^4)} + |1_x^{(1)}\rangle|1_z\rangle^{\otimes(r+r^3)}|1_x\rangle^{\otimes(r^2+r^4)} + \dots). \quad (\text{S.30})$$

Again, as h is even, the procedure ends with another complete layer and the full state is

$$|\psi\rangle = \frac{1}{\sqrt{2}^{r+r^3+\dots+r^{h-1}}} (|0_x^{(1)}\rangle(|0_z\rangle^{\otimes(r+r^3+\dots+r^{h-1})}|0_x\rangle^{\otimes r^2+\dots+r^h} + |1_z\rangle^{\otimes(r+\dots+r^{h-1})}|1_x\rangle^{\otimes r^2+\dots+r^h}). \quad (\text{S.31})$$

Hence the exponent γ in this case reads

$$\gamma = -1 + r + r^3 + \dots + r^{h-1}. \quad (\text{S.32})$$

• **h even $\rightarrow h+1$ odd, r odd**

When another incomplete layer is added, its $|0_x\rangle$ states couple the to $|0_x\rangle$ states of the previous (complete layer). This will transform the latter into $|0_z\rangle$ or $|1_z\rangle$ and generate another fractal of GHZ states. Hence the state from Eq. (S.27) into

$$|\psi\rangle = \frac{1}{\sqrt{2}^{r+r^3+\dots+r^{h-1}+r^{h+1}}} (|0_x^{(1)}\rangle|0_z\rangle^{\otimes(r+r^3+\dots+r^{h-1}+r^h)}|0_x\rangle^{\otimes r^{h+1}} + |1_x^{(1)}\rangle|1_z\rangle^{\otimes(r+\dots+r^{h-1}+r^h)}|1_x\rangle^{\otimes r^{h+1}})|0_x\rangle^{\otimes(r^2+\dots+r^{h-2})}. \quad (\text{S.33})$$

Hence the GHZ coherence in this case is

$$\gamma = -1 + r + r^2 + r^3 + \dots + r^{h-1} + r^{h+1}. \quad (\text{S.34})$$

• **h even $\rightarrow h+1$ odd, r even**

Note that the same argument applies to r even, because these two cases do not differ with respect to the last complete layer. Hence the state upon the addition of the $h+1$ -th incomplete layer will read

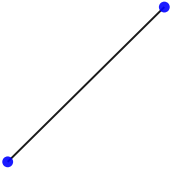
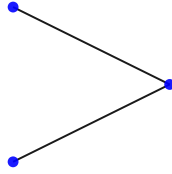
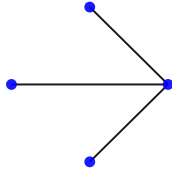
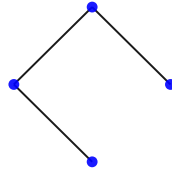
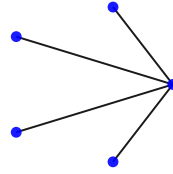
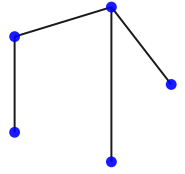
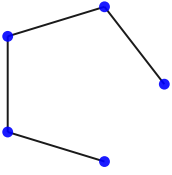
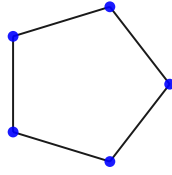
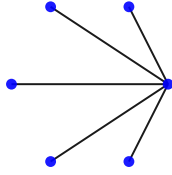
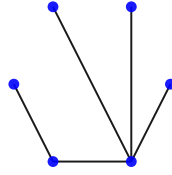
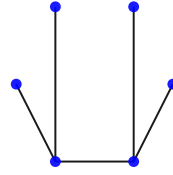
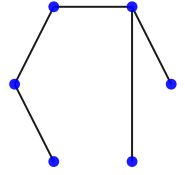
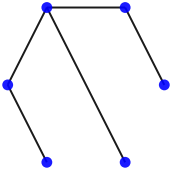
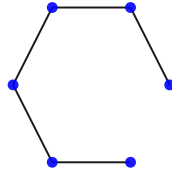
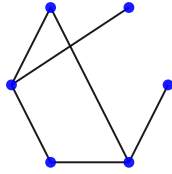
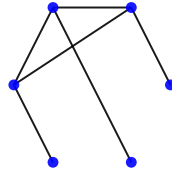
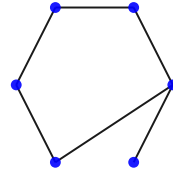
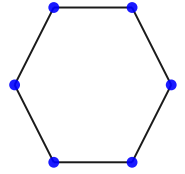
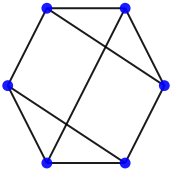
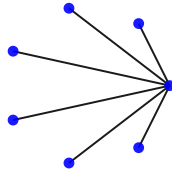
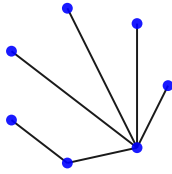
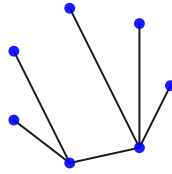
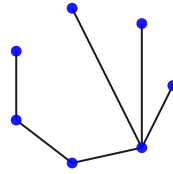
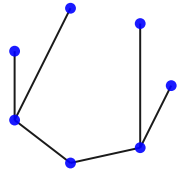
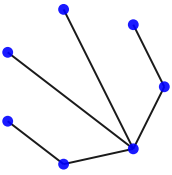
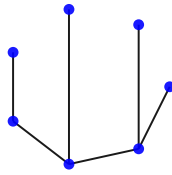
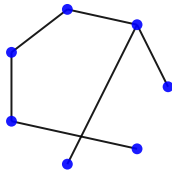
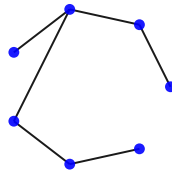
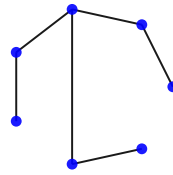
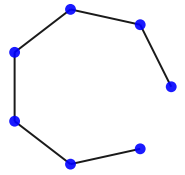
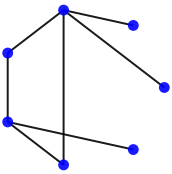
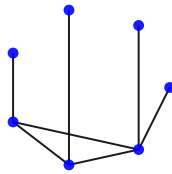
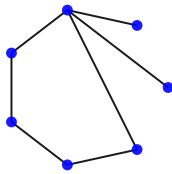
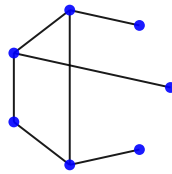
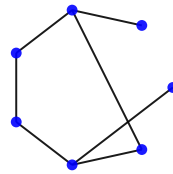
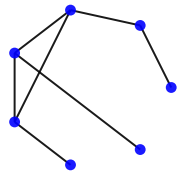
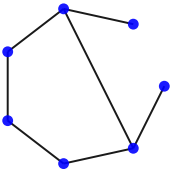
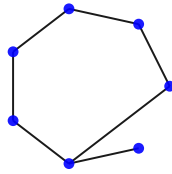
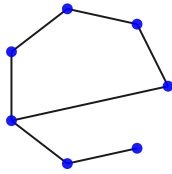
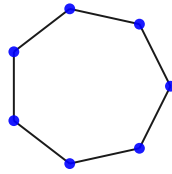
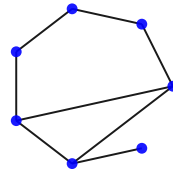
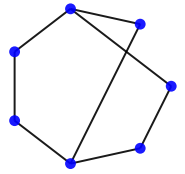
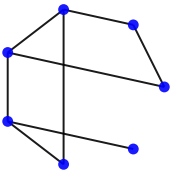
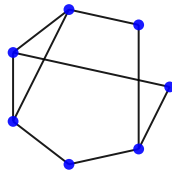
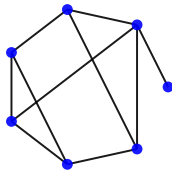
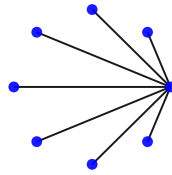
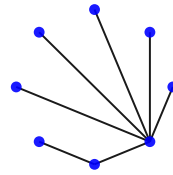
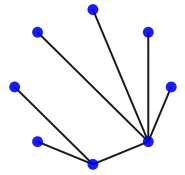
$$|\psi\rangle = \frac{1}{\sqrt{2}^{r+r^3+\dots+r^{h-1}+r^{h+1}}} (|0_x^{(1)}\rangle(|0_z\rangle^{\otimes(r+r^3+\dots+r^{h-1}+r^h)}|0_x\rangle^{\otimes r^2+\dots+r^{h-2}+r^{h+1}} + |1_z\rangle^{\otimes(r+\dots+r^{h-1}+r^h)}|1_x\rangle^{\otimes r^2+\dots+r^{h-2}+r^{h+1}}). \quad (\text{S.35})$$

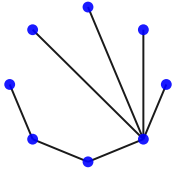
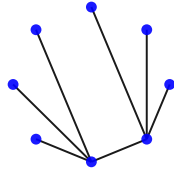
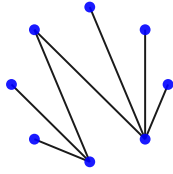
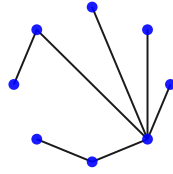
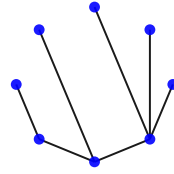
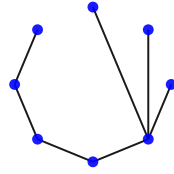
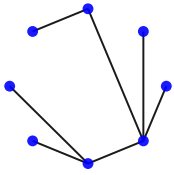
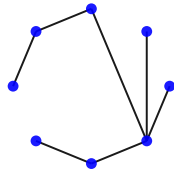
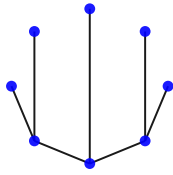
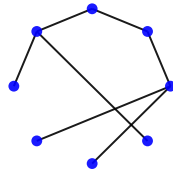
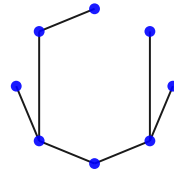
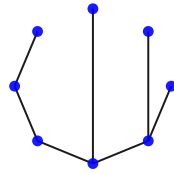
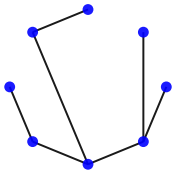
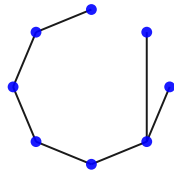
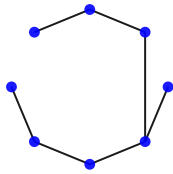
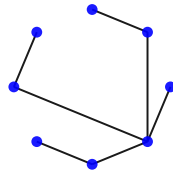
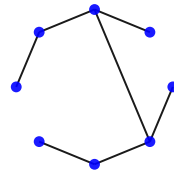
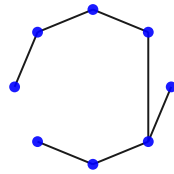
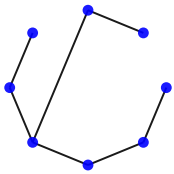
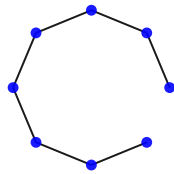
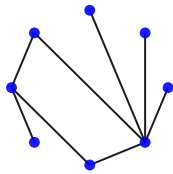
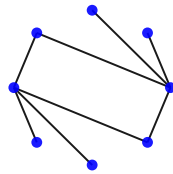
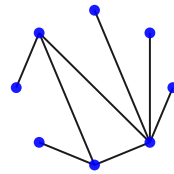
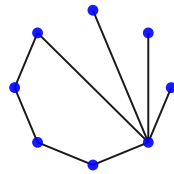
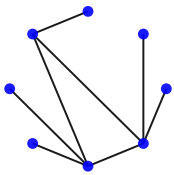
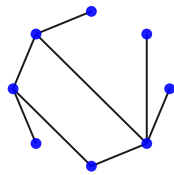
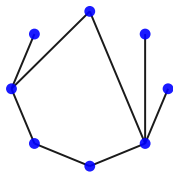
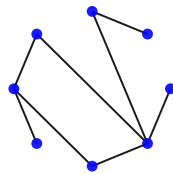
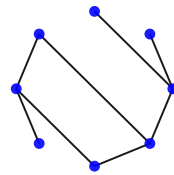
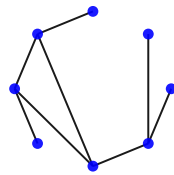
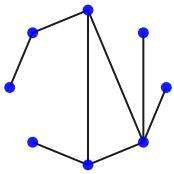
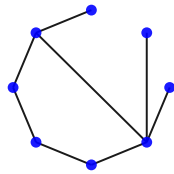
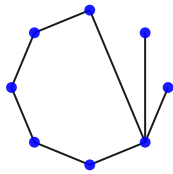
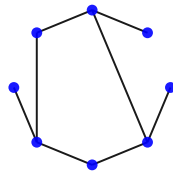
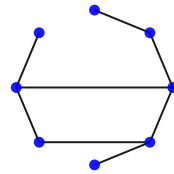
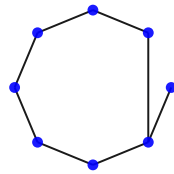
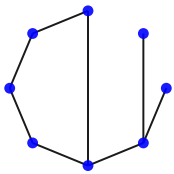
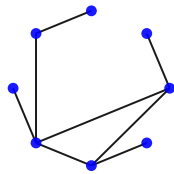
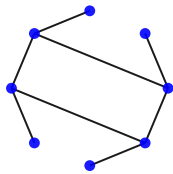
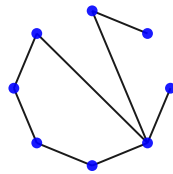
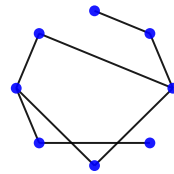
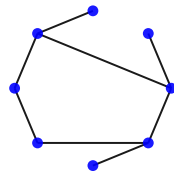
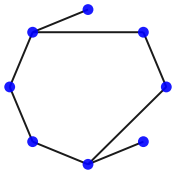
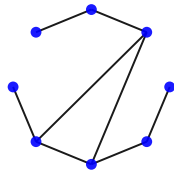
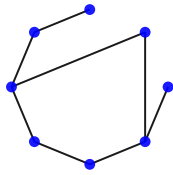
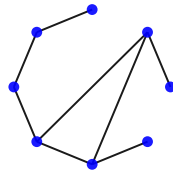
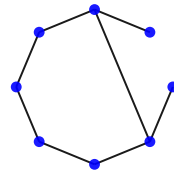
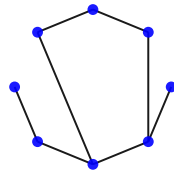
Hence γ in this case reads

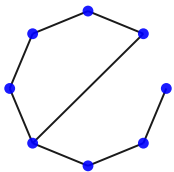
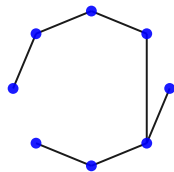
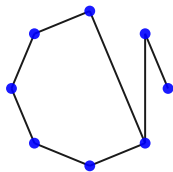
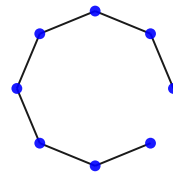
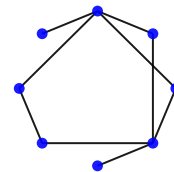
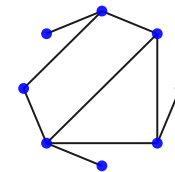
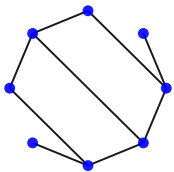
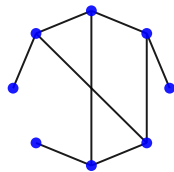
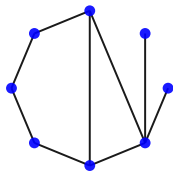
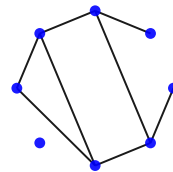
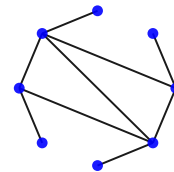
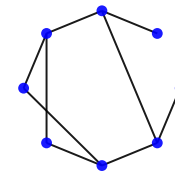
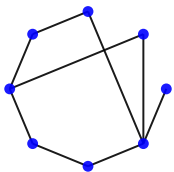
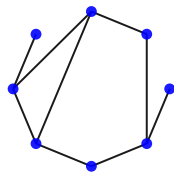
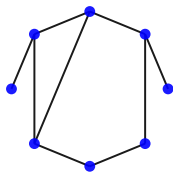
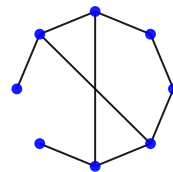
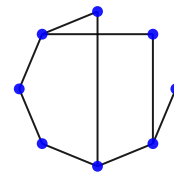
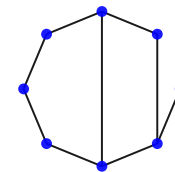
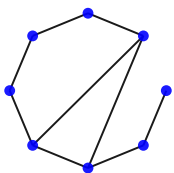
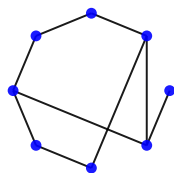
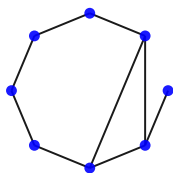
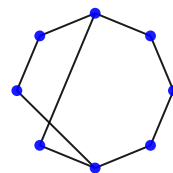
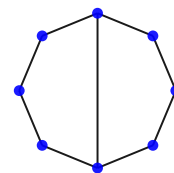
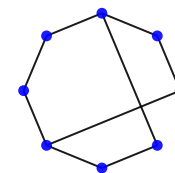
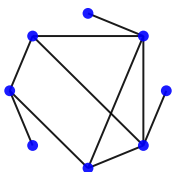
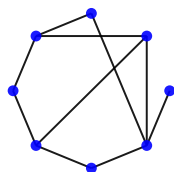
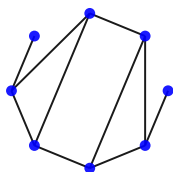
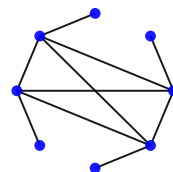
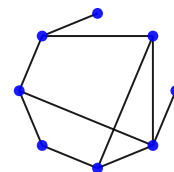
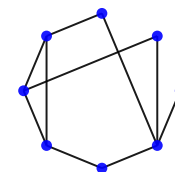
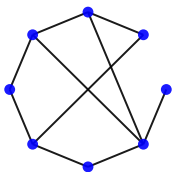
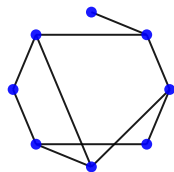
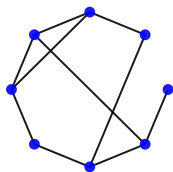
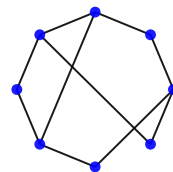
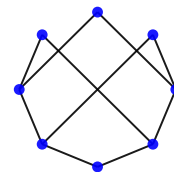
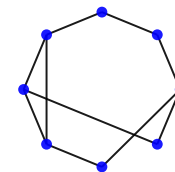
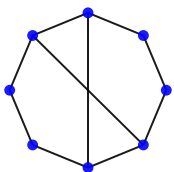
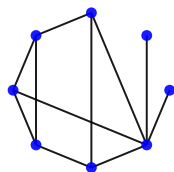
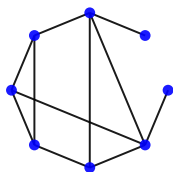
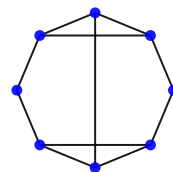
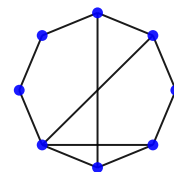
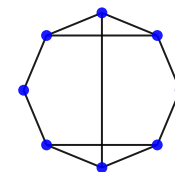
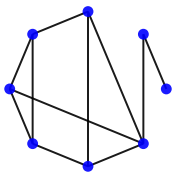
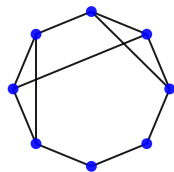
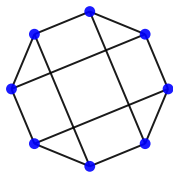
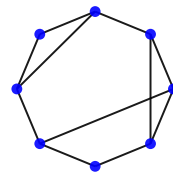
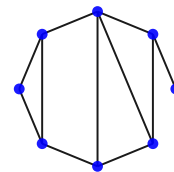
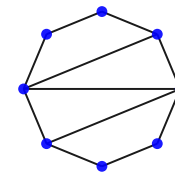
$$\gamma = -1 + r + r^3 + \dots + r^{h-1} + r^{h+1}. \quad (\text{S.36})$$

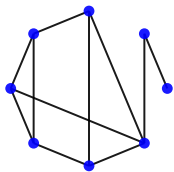
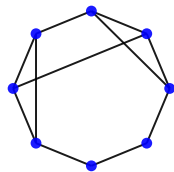
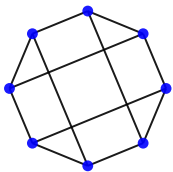
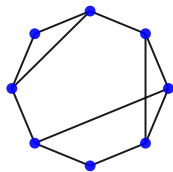
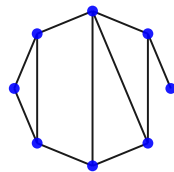
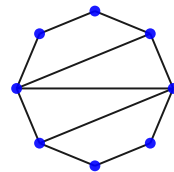
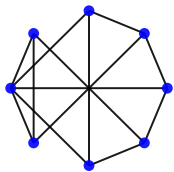
NON-EQUIVALENT CLASSES UNDER LOCAL UNITARIES AND GRAPH ISOMORPHISMS

All connected graph states with up to $L = 8$ qubits can be classified into 146 non-equivalent classes under local unitary transformations and graph isomorphisms [72–74]. Below, we present exponent γ for each such a class representant (graphs enumeration adapted from [72–74]).

No. 1 | $\gamma = 0$ No. 2 | $\gamma = 0$ No. 3 | $\gamma = 0$ No. 4 | $\gamma = 1$ No. 5 | $\gamma = 0$ No. 6 | $\gamma = 1$ No. 7 | $\gamma = 2$ No. 8 | $\gamma = 3$ No. 9 | $\gamma = 0$ No. 10 | $\gamma = 1$ No. 11 | $\gamma = 1$ No. 12 | $\gamma = 2$ No. 13 | $\gamma = 2$ No. 14 | $\gamma = 2$ No. 15 | $\gamma = 3$ No. 16 | $\gamma = 2$ No. 17 | $\gamma = 3$ No. 18 | $\gamma = 3$ No. 19 | $\gamma = 3$ No. 20 | $\gamma = 0$ No. 21 | $\gamma = 1$ No. 22 | $\gamma = 1$ No. 23 | $\gamma = 2$ No. 24 | $\gamma = 2$ No. 25 | $\gamma = 2$ No. 26 | $\gamma = 2$ No. 27 | $\gamma = 2$ No. 28 | $\gamma = 3$ No. 29 | $\gamma = 2$ No. 30 | $\gamma = 3$ No. 31 | $\gamma = 3$ No. 32 | $\gamma = 2$ No. 33 | $\gamma = 3$ No. 34 | $\gamma = 3$ No. 35 | $\gamma = 3$ No. 36 | $\gamma = 2$ No. 37 | $\gamma = 3$ No. 38 | $\gamma = 3$ No. 39 | $\gamma = 3$ No. 40 | $\gamma = 4$ No. 41 | $\gamma = 3$ No. 42 | $\gamma = 4$ No. 43 | $\gamma = 4$ No. 44 | $\gamma = 3$ No. 45 | $\gamma = 3$ No. 46 | $\gamma = 0$ No. 47 | $\gamma = 1$ No. 48 | $\gamma = 1$ 

No. 49 | $\gamma = 2$ No. 50 | $\gamma = 1$ No. 51 | $\gamma = 2$ No. 52 | $\gamma = 2$ No. 53 | $\gamma = 2$ No. 54 | $\gamma = 2$ No. 55 | $\gamma = 2$ No. 56 | $\gamma = 3$ No. 57 | $\gamma = 2$ No. 58 | $\gamma = 2$ No. 59 | $\gamma = 3$ No. 60 | $\gamma = 3$ No. 61 | $\gamma = 2$ No. 62 | $\gamma = 3$ No. 63 | $\gamma = 4$ No. 64 | $\gamma = 3$ No. 65 | $\gamma = 3$ No. 66 | $\gamma = 3$ No. 67 | $\gamma = 3$ No. 68 | $\gamma = 4$ No. 69 | $\gamma = 3$ No. 70 | $\gamma = 3$ No. 71 | $\gamma = 2$ No. 72 | $\gamma = 3$ No. 73 | $\gamma = 2$ No. 74 | $\gamma = 3$ No. 75 | $\gamma = 3$ No. 76 | $\gamma = 4$ No. 77 | $\gamma = 3$ No. 78 | $\gamma = 2$ No. 79 | $\gamma = 2$ No. 80 | $\gamma = 3$ No. 81 | $\gamma = 3$ No. 82 | $\gamma = 4$ No. 83 | $\gamma = 3$ No. 84 | $\gamma = 4$ No. 85 | $\gamma = 3$ No. 86 | $\gamma = 3$ No. 87 | $\gamma = 3$ No. 88 | $\gamma = 4$ No. 89 | $\gamma = 3$ No. 90 | $\gamma = 3$ No. 91 | $\gamma = 3$ No. 92 | $\gamma = 3$ No. 93 | $\gamma = 4$ No. 94 | $\gamma = 3$ No. 95 | $\gamma = 4$ No. 96 | $\gamma = 3$ 

No. 97 | $\gamma = 4$ No. 98 | $\gamma = 3$ No. 99 | $\gamma = 4$ No. 100 | $\gamma = 4$ No. 101 | $\gamma = 4$ No. 102 | $\gamma = 3$ No. 103 | $\gamma = 4$ No. 104 | $\gamma = 2$ No. 105 | $\gamma = 3$ No. 106 | $\gamma = 4$ No. 107 | $\gamma = 3$ No. 108 | $\gamma = 3$ No. 109 | $\gamma = 4$ No. 110 | $\gamma = 4$ No. 111 | $\gamma = 3$ No. 112 | $\gamma = 3$ No. 113 | $\gamma = 4$ No. 114 | $\gamma = 4$ No. 115 | $\gamma = 4$ No. 116 | $\gamma = 4$ No. 117 | $\gamma = 4$ No. 118 | $\gamma = 5$ No. 119 | $\gamma = 4$ No. 120 | $\gamma = 4$ No. 121 | $\gamma = 2$ No. 122 | $\gamma = 4$ No. 123 | $\gamma = 3$ No. 124 | $\gamma = 3$ No. 125 | $\gamma = 3$ No. 126 | $\gamma = 4$ No. 127 | $\gamma = 4$ No. 128 | $\gamma = 3$ No. 129 | $\gamma = 3$ No. 130 | $\gamma = 4$ No. 131 | $\gamma = 4$ No. 132 | $\gamma = 4$ No. 133 | $\gamma = 4$ No. 134 | $\gamma = 3$ No. 135 | $\gamma = 3$ No. 136 | $\gamma = 4$ No. 137 | $\gamma = 4$ No. 138 | $\gamma = 4$ No. 139 | $\gamma = 4$ No. 140 | $\gamma = 4$ No. 141 | $\gamma = 3$ No. 142 | $\gamma = 4$ No. 143 | $\gamma = 4$ No. 144 | $\gamma = 5$ 

No. 139 | $\gamma = 4$ No. 140 | $\gamma = 4$ No. 141 | $\gamma = 3$ No. 142 | $\gamma = 4$ No. 143 | $\gamma = 4$ No. 144 | $\gamma = 5$ No. 145 | $\gamma = 4$ No. 146 | $\gamma = 4$ 